Understanding the reentrant superconducting phase diagram of the iron pnictide $Ca_4Al_2O_6Fe_2(As_{1-x}P_x)_2$: First-principles calculations

Hidetomo Usui,[1] Katsuhiro Suzuki,[2] Kazuhiko Kuroki,[1] Nao Takeshita,[3] Parasharam Maruti Shirage,[3] Hiroshi Eisaki,[3] and Akira Iyo[3]

[1]*Department of Physics, Osaka University, 1-1 Machikaneyama, Toyonaka, Osaka 560-0043, Japan*

[2]*Department of Engineering Science, The University of Electro-Communication, Chofu, Tokyo 182-8585, Japan*

[3]*National Institute of Advanced Industrial Science and Technology (AIST), Central-2, 1-1-1, Umezono, Tsukuba, Ibaraki 305-8568, Japan*

(Received 19 April 2013; published 31 May 2013)

Recently, a very rich phase diagram has been obtained for an iron-based superconductor $Ca_4Al_2O_6Fe_2(As_{1-x}P_x)_2$. It has been revealed that nodeless ($x \sim 0$) and nodal ($x = 1$) superconductivity are separated by an antiferromagnetic phase. Here we study the origin of this peculiar phase diagram using a five orbital model constructed from first-principles band calculation, and applying the fluctuation exchange approximation assuming spin-fluctuation-mediated pairing. At $x = 1$, there are three hole Fermi surfaces, but the most inner one around the wave vector (0,0) has strong $d_{X^2-Y^2}$ orbital character, unlike in LaFeAsO, where the most inner Fermi surface has $d_{XZ/YZ}$ character. Since the Fermi surfaces around (0,0), $(\pi,0)$, and (π,π) all have $d_{X^2-Y^2}$ orbital character, the repulsive pairing interaction mediated by the spin fluctuations gives rise to a frustration in momentum space, thereby degrading superconductivity despite the bond angle being close to the regular tetrahedron angle. As x decreases and the bond angle is reduced, the inner hole Fermi surface disappears, but the frustration effect still remains because the top of the band with $d_{X^2-Y^2}$ character lies close to the Fermi level. On the other hand, the loss of the Fermi surface itself gives rise to a very good nesting of the Fermi surface because the number of electron and hole Fermi surfaces are now the same. The pairing interaction frustration and the good nesting combined favors antiferromagnetism over superconductivity. Finally for x close to 0, the band sinks far below the Fermi level, reducing the frustration effect, so that superconductivity is enhanced. There, the Fermi surface nesting is also lost to some extent, once again favoring superconductivity over antiferromagnetism. To see whether the present theoretical scenario is consistent with the actual nature of the competition between superconductivity and antiferromagnetism, we also perform hydrostatic pressure experiment for $Ca_4Al_2O_6Fe_2(As_{1-x}P_x)_2$. In the intermediate x regime where antiferromagnetism occurs at ambient pressure, applying hydrostatic pressure smears out the antiferromagnetic transition, but superconductivity does not take place. This supports our scenario that superconductivity is suppressed by the momentum space frustration in the intermediate x regime, apart from the presence of the antiferromangnetism.

DOI: 10.1103/PhysRevB.87.174528 PACS number(s): 74.70.Xa, 74.20.Rp, 74.62.Fj

I. INTRODUCTION

The discovery of the iron-based superconductors has given great impact not only because of the high T_c, but also because it raises a fundamental question on the pairing mechanism in a class of high T_c materials other than the cuprates.[1,2] In fact, a spin-fluctuation-mediated pairing mechanism was proposed right after the discovery of superconductivity.[3,4] One interesting and important feature of the iron-based superconductors is the relationship between the superconducting transition temperature and the lattice structure, in particular, the Fe-Pn (Pn:Pnictogen) positional relationship.[5,6] Lee *et al.* have experimentally shown that T_c systematically varies with the Fe-Pn-Fe bond angle, and takes its maximum around 109°, at which the pnictogen atoms form a regular tetrahedron.[5] On the other hand, the strength of the low-lying spin fluctuation seems to be stronger for materials with bond angle smaller than the regular tetrahedron angle, i.e., those materials with moderate to low T_c (Refs. 7–11).

$Ca_4Al_2O_6Fe_2As_2$ is particularly interesting in this context. This material was synthesized by Shirage *et al.*[12] as a variation of a series of materials that have thick perovskite layers in between FeAs layers.[13] This material is particularly interesting from the lattice structure viewpoint in that it has a very small Fe-As-Fe bond angle of 102°. It has been revealed by NMR experiment[7] in the normal state that the spin fluctuation is very strong in this material despite the moderate T_c of about 28 K. The $1/T_1$ measurement in the superconducting state suggests that the gap is fully open with a sign change between electron and hole Fermi surfaces, namely, a fully gapped $s\pm$ state.[7]

Theoretically, we have previously explained this correlation among the lattice structure, the spin fluctuations, and the superconducting T_c/gap structure within the spin-fluctuation-mediated pairing scenario using a five orbital model obtained for the hypothetical lattice structure of LaFeAsO (Refs. 14 and 15). We have concluded that superconductivity is strongly affected by the Fermi surface multiplicity, and the spin fluctuation is strongly affected by the hole Fermi surface around the wave vector (π,π) in the unfolded Brillouin zone. It has been found that the number of Fermi surface is controlled by the Fe-Pn-Fe bond angle or the pnictogen height. When the bond angle is large (low pnictogen height), two hole Fermi surfaces around the wave vector (0,0) are present. In this case, a low T_c nodal s-wave paring or d-wave paring takes place.[15–18] As the bond angle α decreases, the hole Fermi surface appears around (π,π), and we now have three hole Fermi surfaces. This is what has been noticed as an effect of increasing the pnictogen height.[15,19,20] the interaction between the electron and the hole

Fermi surfaces gives rise to a high T_c $s\pm$-wave paring, where the gap is fully open but changes sign between electron and hole Fermi surfaces as was first proposed by the authors of Ref. 4. Upon reducing α even further (and thus increasing the high pnictogen height), the inner hole Fermi surface around (0,0) disappears, and again there are only two hole Fermi surfaces. Here, the good Fermi surface nesting gives rise to a strong spin fluctuation, while the superconducting T_c of the gapped $s\pm$ state remains to be moderate because of the reduction of the scattering processes. Thus, superconductivity is optimized in the intermediate bond angle regime around 110°, where the Fermi surface multiplicity is maximized.

However, there are some experimental observations that seem to be beyond the understanding of the above-mentioned theory. For example, the phosphide version of this 42 622 material $Ca_4Al_2O_6Fe_2P_2$ has a lower T_c of 17 K (Ref. 12) although the bond angle is nearly 109°, which is very close to the regular tetrahedron bond angle. In the phosphides, the Fe-Pn bond length is generally reduced compared to the arsenides, so the density of states tends to be smaller. Therefore, the phosphides and the arsenides do not have to obey the same T_c vs. bond angle dependence. Still, there seems to be some effect that suppresses T_c in $Ca_4Al_2O_6Fe_2P_2$, considering the fact that (i) $T_c = 17$ K is nearly the same as $Sr_4Sc_2O_6Fe_2P_2$ with a much larger bond angle;[13] (ii) the band structure calculation for $Ca_4Al_2O_6Fe_2P_2$ by Kosugi *et al.*[21] shows that the number of hole Fermi surfaces is three, i.e., the inner Fermi surface is not lost as opposed to $Ca_4Al_2O_6Fe_2As_2$, and the Fermi surface multiplicity is maximized; and (iii) an NMR experiment for $Ca_4Al_2O_6Fe_2P_2$ suggests the presence of nodes in the superconducting gap (or a very small gap at some portions of the Fermi surface).[22]

Quite recently, an interesting observation has been made for $Ca_4Al_2O_6Fe_2(As_{1-x}P_x)_2$, an isovalent doping material, where As is (partially) replaced by P. As mentioned above, the end materials at $x = 0$ and $x = 1$ are both superconductors. In between these two phases, antiferromagnetism takes place in the intermediate regime of the P content x, and separates the two superconductivity phases of $x \sim 0$[12] and $x \sim 1$ (Refs. 22 and 23). Therefore, $Ca_4Al_2O_6Fe_2(As_{1-x}P_x)_2$ varies from a fully gapped superconducting state to an antiferromagnetism and finally to a nodal superconducting state.

In this paper, we study this peculiar behavior of superconductivity and antiferromagnetism in $Ca_4Al_2O_6Fe_2(As_{1-x}P_x)_2$ from a lattice structure and band structure point of view. We calculate the band structure of the hypothetical lattice structure of $Ca_4Al_2O_6Fe_2As_2$ and construct an effective five band model exploiting the maximally localized Wannier orbitals. In varying the bond angle in a wide range while fixing the bond length, we find that the most inner hole Fermi surface around the wave vector (0,0) in the unfolded Brillouin zone changes its orbital character from XZ/YZ to $X^2 - Y^2$ just before it disappears. Then the Fermi surfaces around the wave vectors (0,0), $(\pi,0)$, and (π,π) will all (partially) have $X^2 - Y^2$ orbital character. This is the Fermi surface configuration for $Ca_4Al_2O_6Fe_2P_2$. Since the spin-fluctuation-mediated pairing interaction tends to change the sign of the superconducting gap between portions of the Fermi surface having similar orbital character, this will give rise to a frustration in momentum space, degrading superconductivity. We also explain the competition between superconductivity and antiferromagnetism in $Ca_4Al_2O_6Fe_2(As_{1-x}P_x)_2$. Around the intermediate region of x, the most inner Fermi surface is lost, but the top of the band still lies close to the Fermi level. In this situation, the momentum space frustration effect is still strong, and the superconductivity is suppressed. At the same time and independently, the Fermi surface itself is nearly perfectly nested since there are now two electron and two hole Fermi surfaces with the same total area (for zero doping). For smaller x, the band that gives rise to the frustration sinks far below the Fermi level, and superconductivity again takes over antiferromagnetism.

To see whether the present theoretical scenario is consistent with the actual nature of the superconductivity-antiferromagnetism competition in the present material, we also a perform hydrostatic pressure experiment. In the intermediate x regime, superconductivity does not take place under pressure although the pressure smears out the antiferromagnetic transition. This experiment further supports our view that in the intermediate x regime superconductivity is suppressed by some origin other than the antiferromagnetism itself, which in our view is the momentum space frustration.

II. BAND STRUCTURE

A. Original lattice structure

We first calculate the band structure of $Ca_4Al_2O_6Fe_2As_2$, which was first performed by the authors of Ref. 24, and compare it to that of LaFeAsO. We adopt the lattice structure determined experimentally,[12] where the Fe-As-Fe bond angle α is 102° and the pnictogen height $h_{\rm Pn}$ measured from the iron plane is 1.5 Å. The first-principles band calculation is performed using the QUANTUM ESPRESSO package,[25] and we construct a five orbital tight-binding Hamiltonian[3] exploiting the maximally localized Wannier functions.[26] The five Wannier orbitals consist mainly of Fe $3d$ and As $4p$ orbitals, and these orbitals have five different symmetries (d_{XY}, d_{YZ}, d_{ZX}, $d_{3Z^2-R^2}$, and $d_{X^2-Y^2}$), where X,Y refer to the direction of rotated by 45° from the Fe-Fe direction x,y. The multi-orbital tight binding Hamiltonian is expressed as

$$H_0 = \sum_{\sigma} \sum_{i,\mu} \varepsilon_{\mu} c^{\dagger}_{i\mu\sigma} c_{i\mu\sigma} + \sum_{\sigma} \sum_{ij,\mu\nu} t^{\mu\nu}_{ij} c^{\dagger}_{i\mu\sigma} c_{j\nu\sigma}, \qquad (1)$$

where $t^{\mu\nu}_{ij}$ is the hopping, i,j denote the sites, and μ,ν specify the orbitals. We define the band filling n as the number of electrons per site, where $n = 6$ refers to the nondoped case. The Fermi surfaces shown in Fig. 1 are those for the $k_z = 0$ plane and $n = 6$.

As pointed out in Ref. 24, a large difference between the band structure of the two materials is the number of hole Fermi surfaces. In LaFeAsO, there are two hole Fermi surfaces around the wave vector $(k_x,k_y) = (0,0)$ originating from the XZ/YZ orbitals, and one hole Fermi surface around (π,π) originating from the $X^2 - Y^2$ orbital. In $Ca_4Al_2O_6Fe_2As_2$ by contrast, one of the hole Fermi surfaces around (0,0) (α_1) is missing. This difference is due to the position of the upper portion of the $X^2 - Y^2$ band along $(0,0,0) - (0,0,\pi)$ indicated by the short arrows in Fig. 1. This band lies above the XZ/YZ bands in LaFeAsO, while it lies below the XZ/YZ bands in $Ca_4Al_2O_6Fe_2As_2$. We will come back to

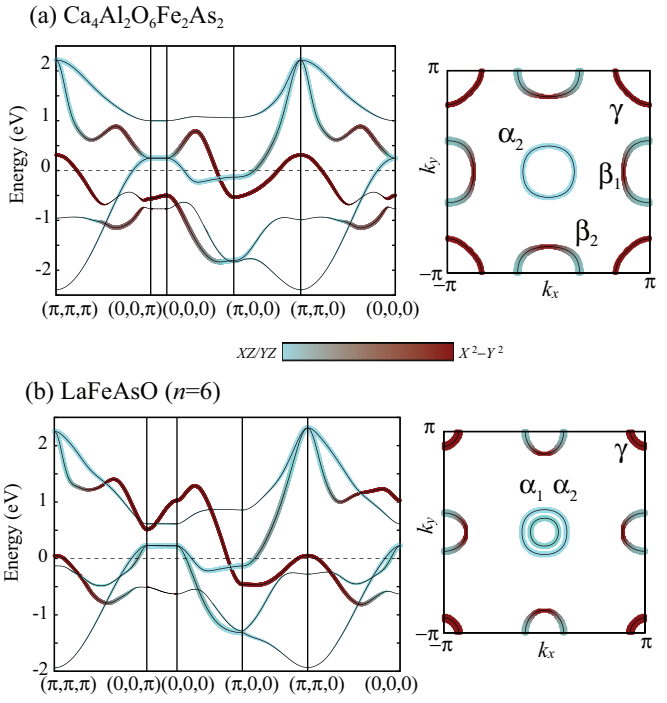

FIG. 1. (Color online) The band structure and the Fermi surface of (a) LaFeAsO and (b) $Ca_4Al_2O_6Fe_2As_2$. The thickness of the lines represents the weight of the X^2-Y^2 or XZ/YZ orbital characters.

this point in more detail in the next subsection. Another large difference between the two materials is the strength of the two dimensionality. The band structure of $Ca_4Al_2O_6Fe_2As_2$ has strong two dimensionality due to the large block layer, namely, the dispersion of the upper X^2-Y^2 band along $(0,0,0)-(0,0,\pi)$ is much smaller than in LaFeAsO.

B. Bond angle variation

As was done in Refs. 14 and 24, we discuss the bond angle dependence of the band structure. Before going into $Ca_4Al_2O_6Fe_2As_2$, we summarize the bond angle variation of the band structure of LaFeAsO, which was discussed in detail in Refs. 14 and 27. In Fig. 2, we show the band structure of LaFeAsO for the hypothetical lattice structures with smaller bond angles than in the original lattice structure with 113°. The lower portion of the X^2-Y^2 band around (π,π) rises up upon reducing the bond angle, and at the same time the upper X^2-Y^2 band along $(0,0,0)-(0,0,\pi)$ comes down and partially sinks below the XZ/YZ bands at 108°. This variation of the bands is schematically summarized in Fig. 3.[27] When the upper X^2-Y^2 band sinks below the XZ/YZ bands, the reconstruction of the band structure takes place, and one of the hole Fermi surface is lost for sufficiently small bond angle [configuration (d)]. It is important to note that just before the α_1 hole Fermi surface is lost, the X^2-Y^2 orbital character strongly mixes into the α_1 Fermi surface [configuration (c)]. Due to the three-dimensional dispersion of the upper X^2-Y^2 band in LaFeAsO, the disappearance of the α_1 Fermi surface is k_z dependent, so that the Fermi surface becomes three dimensional for a certain bond angle regime, as shown in the left panel of Fig. 2(c). Even when the Fermi surface itself is two dimensional, the orbital character can change along the k_z

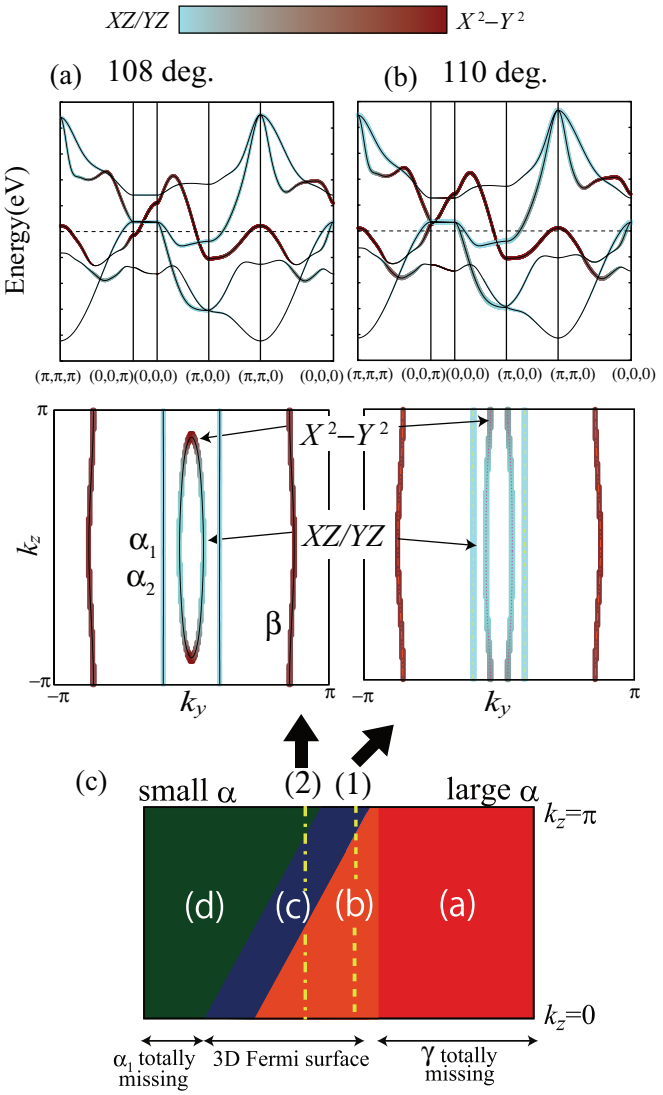

FIG. 2. (Color online) The band structure (top) and the vertical cut of the Fermi surface of LaFeAsO for hypothetical lattice structures with (a) $\alpha = 108°$ or (b) $\alpha = 110°$. The thickness of the lines represents the weight of the X^2-Y^2 or XZ/YZ orbital characters. (c) A schematic figure representing the band structure/Fermi surface configuration in the α-k_z plane. (a)–(d) correspond to the configurations shown in Fig. 3.

direction as shown in the right panel. This k_z dependence of the Fermi surface configuration of LaFeAsO is schematically summarized in Fig. 2(c).[27]

Bearing this in mind, we now move on to $Ca_4Al_2O_6Fe_2As_2$. Although this was analyzed in detail in Ref. 24, here we put more focus on the orbital character of the most inner hole Fermi surface. In Fig. 4, we show the band structure variation upon decreasing the bond angle from 120° to 100°. (The original lattice structure is 102°.) It is interesting to note that most portion of the upper X^2-Y^2 band sinks below the XZ/YZ bands even at 120°. Therefore, a Fermi surface configuration that does not occur in LaFeAsO takes place. This is schematically shown in Fig. 3 as configuration (c′). As the bond angle is reduced, the γ Fermi surface around (π,π) appears, followed by the disappearance of the α_1 hole

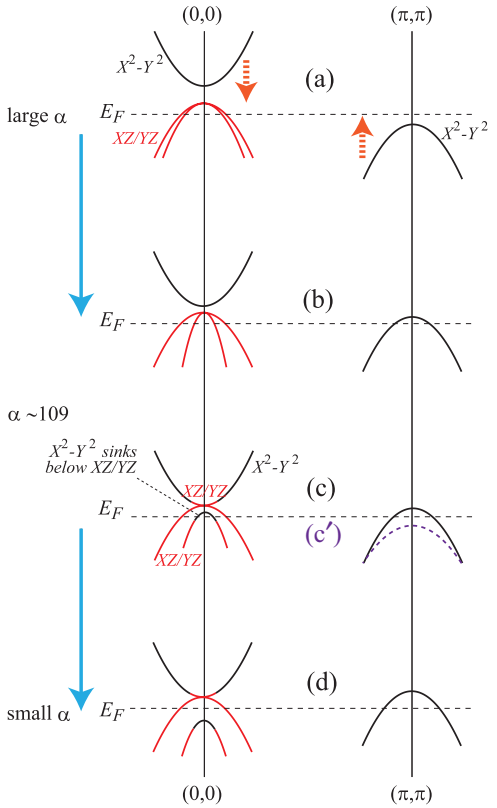

FIG. 3. (Color online) A schematic figure of the band structure variation against the bond angle α. The solid black (solid red) portions indicate the bands with strong $X^2 - Y^2$ (XZ/YZ) orbital character.

Fermi surface. This disappearance occurs in a narrow bond angle regime between 111° to 109° due to the strong two dimensionality. The Fermi surface configuration variation for $Ca_4Al_2O_6Fe_2As_2$ is summarized in Fig. 4(b). Here it is important to note that configuration (b) in Fig. 3 does not appear in this case, namely, the inner α_1 hole Fermi surface always has some mixture of $X^2 - Y^2$ orbital component in the regime where three hole Fermi surfaces exist. As we shall see, this will affect the conclusion in our previous paper,[14] i.e., superconductivity is optimized in the bond angle regime in which the multiplicity of the hole Fermi surface is maximized.

C. Height variation

Upon partially replacing As by P in $Ca_4Al_2O_6Fe_2(As_{1-x}P_x)_2$, the bond angle reduction is accompanied by the increase in the Fe-Pn bond length. Therefore, the lattice parameter a hardly decreases, while the pnictogen height measured from the iron plane largely decreases from 1.5 to 1.3 Å as the P content x increases from 0 to 1. We show in Fig. 5 the band structure of $Ca_4Al_2O_6Fe_2As_2$ for the hypothetical lattice structures varying the pnictogen height while fixing the lattice parameter a. Here the pnictogen height of 1.3 Å corresponds to $\alpha = 110°$ (close to the lattice structure of $x = 1$) and 1.5 Å to 102° (close to $x = 0$). In addition to the change of the Fermi surface configuration due to the the bond angle variation, the height reduction results in an increase of the band width (suppression of the density of states) due to the reduction of the bond length.[14]

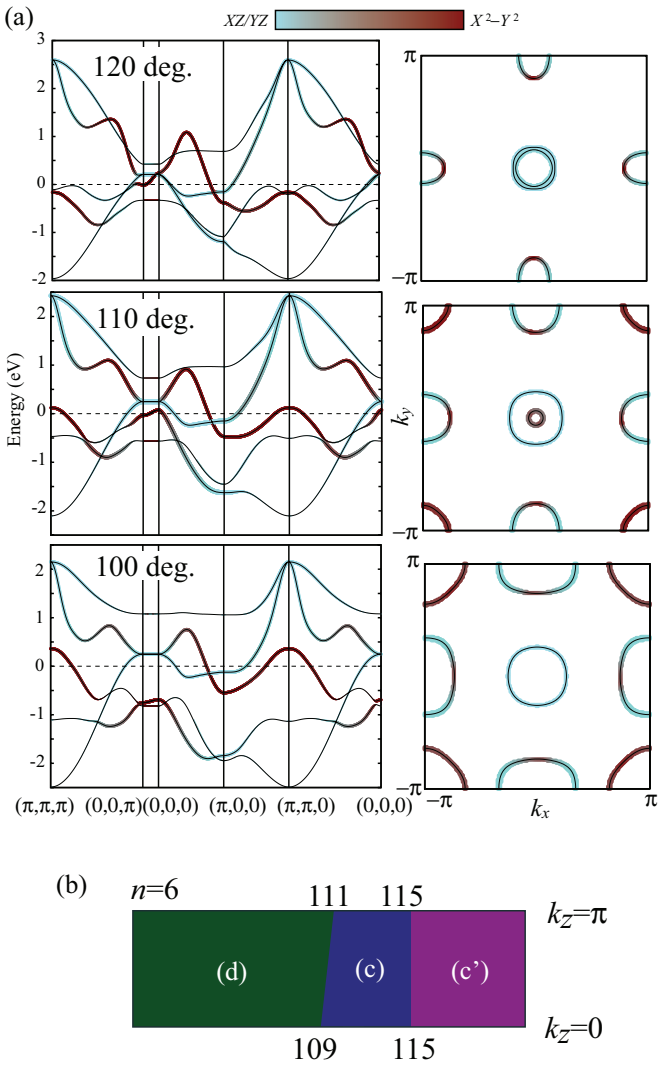

FIG. 4. (Color online) (a) The band structure (left) and the Fermi surface at $k_z = 0$ (right) of $Ca_4Al_2O_6Fe_2As_2$ for hypothetical lattice structures with $\alpha = 120°$, 110°, and 100°. The thickness of the lines represents the weight of the $X^2 - Y^2$ or XZ/YZ orbital characters.

III. SUPERCONDUCTIVITY

A. FLEX approximation

We now move on to the analysis of the spin fluctuation and superconductivity of $Ca_4Al_2O_6Fe_2As_2$. In addition to the tight binding model constructed from first-principles band calculation, we consider the standard multi-orbital interactions, namely, the intraorbital U, the interorbital U', the Hund's coupling J, and the pair hopping interaction J', so the Hamiltonian reads

$$H = H_0 + \sum_i \Bigg(\sum_\mu U_\mu n_{i\mu\uparrow} n_{i\mu\downarrow} + \sum_{\mu>\nu} \sum_{\sigma,\sigma'} U'_{\mu\nu} n_{i\mu\sigma} n_{i\nu\sigma'} - \sum_{\mu\neq\nu} J_{\mu\nu} \boldsymbol{S}_{i\mu} \cdot \boldsymbol{S}_{i\nu} + \sum_{\mu\neq\nu} J'_{\mu\nu} c^\dagger_{i\mu\uparrow} c^\dagger_{i\mu\downarrow} c_{i\nu\downarrow} c_{i\nu\uparrow} \Bigg). \quad (2)$$

We apply the fluctuation exchange (FLEX) approximation[28,29] using the multi-orbital Hubbard Hamiltonian. In FLEX, bubble

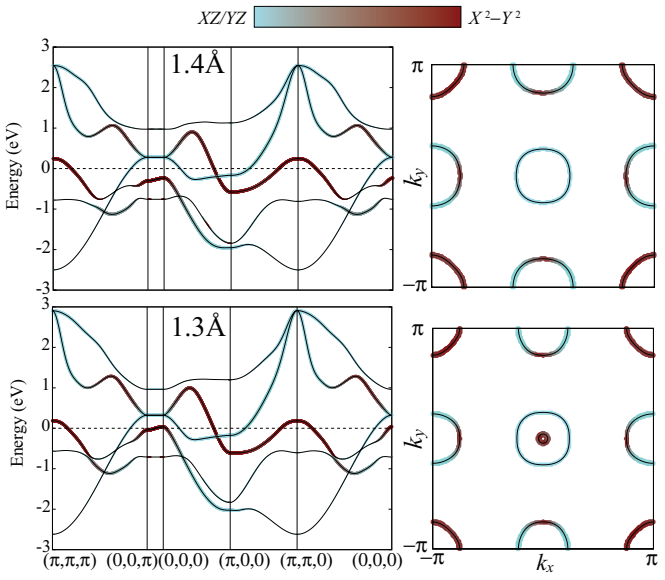

FIG. 5. (Color online) The band structure and the Fermi surface of hypothetical lattice structure in $Ca_4Al_2O_6Fe_2As_2$ with varying pnictogen height while fixing lattice parameter a.

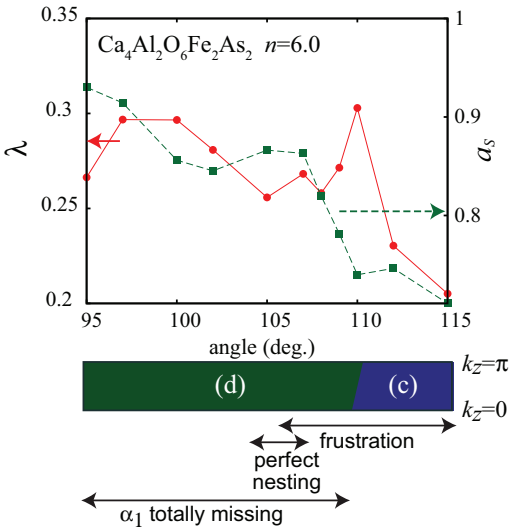

FIG. 6. (Color online) (a) The Eliashberg equation eigenvalue for superconductivity ($s\pm$-wave pairing) (solid line) and the Stoner factor at $(\pi,0)$ (dashed line) against the bond angle for temperature $T = 0.005$. The interaction reduction factor is $f = 0.45$.

and ladder-type diagrams consisting of renormalized Green's functions are summed up to obtain the susceptibilities, which are used to calculate the self-energy. The renormalized Green's functions are then determined self-consistently from the Dyson's equation. The obtained Green's function is plugged into the linearized Eliashberg equation, whose eigenvalue λ reaches unity at the superconducting transition temperature $T = T_c$. Also, to investigate the correlation between superconductivity and magnetism, we obtain the Stoner factor a_S of the antiferromagnetism at the wave vector $(\pi,0)$ in the unfolded Brillouin zone, which is defined as the largest eigenvalue of the matrix $U\chi_0(\mathbf{k} = (\pi,0), i\omega_n = 0)$, where U is the interaction and χ_0 is the irreducible susceptibility matrices, respectively. This value monitors the tendency towards stripe-type antiferromagnetism and the strength of the spin fluctuations at zero energy. Since the three dimensionality is not strong in $Ca_4Al_2O_6Fe_2As_2$, we take a two-dimensional model where we neglect the out-of-plane hopping integrals, and take 32×32 k-point meshes and 4096 Matsubara frequencies.

As for the electron-electron interaction values, we adopt the orbital-dependent interactions as obtained from first-principles calculation in Ref. 30 for $Ca_4Al_2O_6Fe_2As_2$, but multiply all of them by a constant reducing factor f. The reason for introducing this factor is as follows. As has been studied by the authors of Refs. 31–33, the FLEX calculation for models obtained from local-density approximation (LDA) calculations tends to overestimate the effect of the self-energy because LDA already partially takes into account the effect of the self-energy in the exchange-correlation functional. When the electron-electron interactions as large as those evaluated from first principles are adopted in the FLEX calculation, this double counting of the self-energy becomes so large that the band structure largely differs from its original one. In such a case, the spin fluctuations will develop around the wave vector (π,π) rather than $(\pi,0)$, which is in disagreement with the experimental observations. In the present study, we therefore introduce the factor f so as to reduce the electron-electron interactions, while maintaining the relative magnitude between interactions of different orbitals.

B. Bond angle

We show the eigenvalue of the Eliashberg equation λ for the s$\pm$-wave superconductivity and the Stoner factor at $(\pi,0)$ for the hypothetical lattice structure of $Ca_4Al_2O_6Fe_2As_2$ varying the bond angle while fixing the bond length (Fig. 6).

As we decrease the bond angle from115° to 110°, eigenvalue of the Eliashberg equation λ increases, reflecting the appearance of the γ Fermi surface around (π,π). Superconductivity is locally optimized around 110°, but λ immediately goes down for larger bond angle. This is in contrast to the case of LaFeAsO, where λ is broadly maximized around the regular tetrahedron bond angle. This difference can be understood from the comparison between Figs. 2(c) and 4(b). Namely, in the case of $Ca_4Al_2O_6Fe_2As_2$ with hypothetical bond angle, the Fermi surface configuration (b) with the optimal Fermi surface configuration is missing, i.e., in the three Fermi surface regime, α_1 Fermi surface around (0,0) is constructed from a mixture of $X^2 - Y^2$ and XZ/YZ orbital characters. In this configuration, the pair scattering takes place not only at $\sim(\pi,0)$ but also at $\sim(\pi,\pi)$ due to the same orbital character between α_2 and γ Fermi surfaces. Since these Fermi surfaces interact with repulsive pairing interactions, a frustration arises in the sign of the superconducting gap as shown schematically in Fig. 7. In addition to this, there can also be some XZ/YZ component remaining in the α_1 Fermi surface, and this portion tends to change the sign from the β Fermi surfaces, making it another possible factor for the frustration. The effect of the frustration appears in the form of the superconducting gap. In Fig. 8, we show the gap function for the hypothetical lattice structure of $Ca_4Al_2O_6Fe_2As_2$ at the bond angles 110° and 111°. The sign of the gap function on α_1 is positive at 111°, but is very small (barely positive) at 110° (Ref. 34), reflecting the effect of the

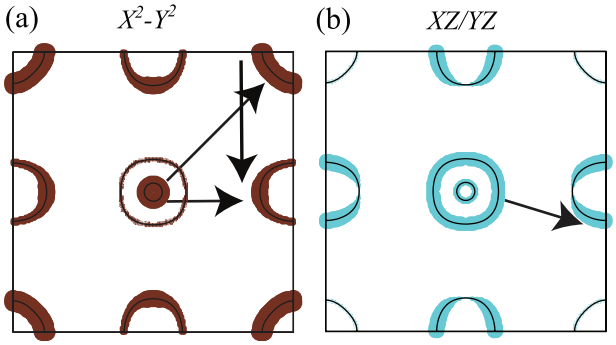

FIG. 7. (Color online) The arrows indicate the wave vector of the dominant pairing interactions for the (a) $X^2 - Y^2$ and (b) XZ/YZ portions of the Fermi surface in the case where the inner hole Fermi surface (α_1) is barely present. In this case, α_1 is a mixture of $X^2 - Y^2$ and XZ/YZ.

frustration. The bond angle of 110° is actually very close to that of $Ca_4Al_2O_6Fe_2P_2$, so the appearance of a very small gap at this bond angle may be related to the nodal gap structure suggested experimentally for $Ca_4Al_2O_6Fe_2P_2$ (Ref. 7). As the bond angle is further reduced, the α_1 Fermi surface disappears, but the effect of the frustration remains strong as far as the top of the α_1 hole band does not sink far below the Fermi level. In fact, the frustration effect can be very strong right after the Fermi surface disappears because the top of this α_1 band (the closest point to the Fermi level) has pure $X^2 - Y^2$ orbital character. Therefore, λ is suppressed around the bond angle of 105°–108°. Meanwhile, the Fermi surface nesting itself becomes very good in this regime because there are now two hole and two electron Fermi surfaces with no doped

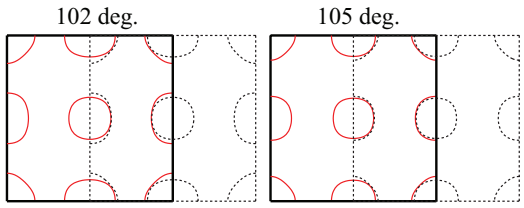

FIG. 9. (Color online) The Fermi surface of $Ca_4Al_2O_6Fe_2As_2$ for the hypothetical lattice structures with $\alpha = 105°$ and 102° (solid line), superposed with the Fermi surface shifted by $(\pi,0)$ (dashed line).

carriers, so that the average area of the hole and the electron Fermi surfaces becomes the same. In particular, around the bond angle of 105°, the nesting becomes nearly perfect, as shown in Fig. 9. Therefore, the Stoner factor at $(\pi,0)$ takes a local maximum around this bond angle. As the bond angle is reduced even further, the $X^2 - Y^2$ band sinks far below the Fermi level and the frustration effect becomes small, so that λ increases once again to a value comparable to that around the local maximum around the regular tetrahedron bond angle. At the same time, the Fermi surface nesting becomes somewhat degraded, and the Stoner factor is reduced. For smaller bond angle <96° (which may not be realistic), the Fermi surface becomes too large, and the superconductivity is degraded. The bottom line here is that superconductivity is favored at around two bond angles 102° and 110°, and antiferromagnetism is favored in the regime in between these angles. This is at least qualitatively consistent with the experimental observations for $Ca_4Al_2O_6Fe_2(As_{1-x}P_x)_2$.

The important point here is that superconductivity is suppressed in the intermediate bond angle regime due to the frustration effect. Apart from this, antiferromagnetism is

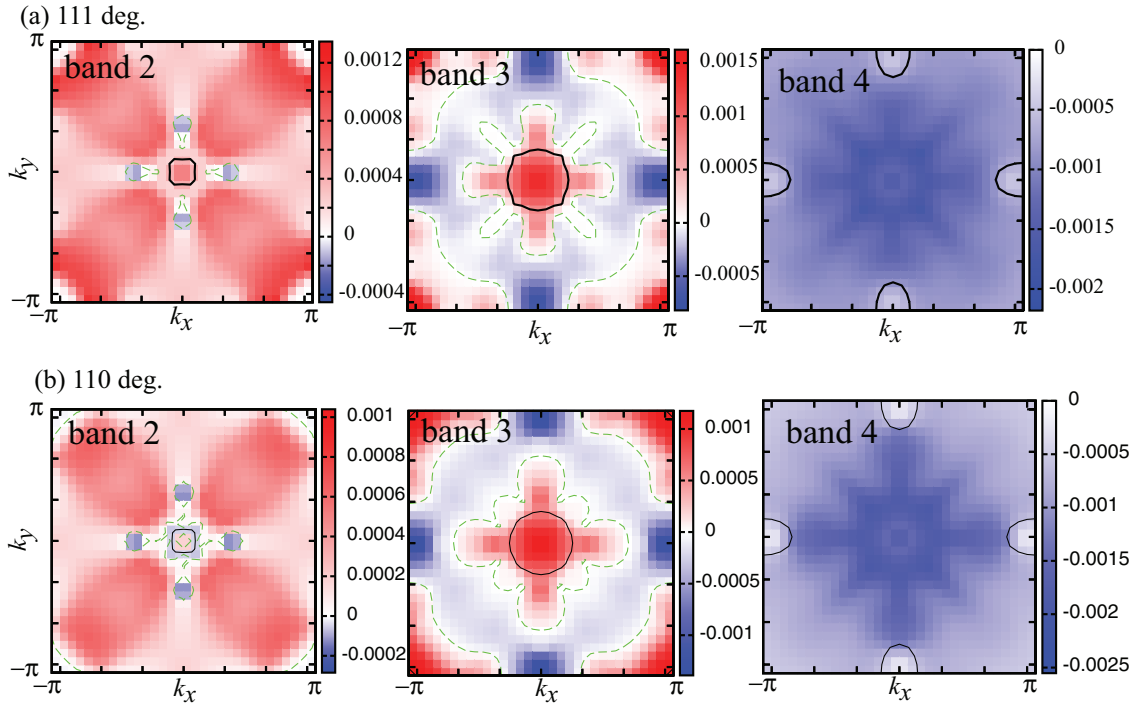

FIG. 8. (Color online) The gap function obtained by FLEX for the hypothetical lattice structures of $Ca_4Al_2O_6Fe_2As_2$. The bond angle α is set to 110° or 111°, while the bond length is fixed at the original value.

favored around this bond angle regime due to a nearly perfect nesting of the Fermi surface.

C. Pnictogen height

We have studied in the previous section the bond angle dependence of superconductivity and the spin fluctuations, and mentioned the possible relation between the calculation results and the experimental observations for $Ca_4Al_2O_6Fe_2(As_{1-x}P_x)_2$. As mentioned previously, the actual lattice structure variation upon replacing As by P is more close to the variance of the pnictogen height h_{Pn} rather than just the bond angle. The increase of the bond length results in an increase in the density of states, generally resulting in an enhancement of both superconductivity and spin fluctuations.[14] In Fig. 10, we show the eigenvalue of the Eliashberg equation and the Stoner factor at $(\pi,0)$ for the hypothetical lattice structure of $Ca_4Al_2O_6Fe_2As_2$ varying solely the pnictogen height h_{Pn}. Around $h_{Pn} = 1.3$–1.35 Å, corresponding to the P content close to unity, the height dependence of λ is weak (or λ is even suppressed with the increase of h_{Pn} for large f), while the Stoner factor rapidly increases with h_{Pn}. This height regime corresponds to the bond angle regime of 110°–108°, where superconductivity is suppressed due to the momentum space frustration, and at the same time antiferromagnetism is favored due to the nearly perfect nesting (Fig. 7). Here in Fig. 10(a), the enhancement of superconductivity by the increase of the density of states is canceled out due to the frustration effect, so that the h_{Pn} dependence of λ is weak. On the other hand, the Stoner factor quickly grows due to the cooperation of the good nesting and the increased density of states. As the pnictogen height increases further beyond 1.35 Å, λ starts to increase rapidly due to the reduction of the frustration and the increase of the density of states, while the Stoner factor tends to saturate because the nearly perfect nesting is degraded. This overall tendency is summarized in a schematic figure in Fig. 10(c).

IV. PRESSURE EXPERIMENT

Our theoretical study so far has shown that in the region where antiferromagnetism appears in the phase diagram, not only antiferromagnetism is enhanced due to the good Fermi surface nesting, but also superconductivity is suppressed due to the momentum space frustration, and these two are independent matters. Since superconductivity is suppressed regardless of whether antiferromagnetism is present or not, superconductivity may not take place even when antiferromagnetism is suppressed by applying pressure, as is often done in other iron-based superconductors.

To actually see this experimentally, we have applied hydrostatic pressure to $Ca_4Al_2O_6Fe_2(As_{1-x}P_x)_2$. The results are shown in Fig. 11. For the end compounds $x = 0$ and $x = 1$, T_c monotonically decreases with increasing pressure. This is most likely due to the decrease in the density of states. For $x = 0.75$, where antiferromagnetism takes place at ambient pressure, superconductivity is not found up to 12 GPa, although the antiferromagnetic transition is smeared out at high pressures. This is in contrast with cases where antiferromagnetism takes place at ambient pressure, but gives way to superconductivity under pressure. The present experimental result supports the scenario that superconductivity in the intermediate x regime is suppressed by momentum space frustration, apart from the presence of the antiferromagnetism itself.

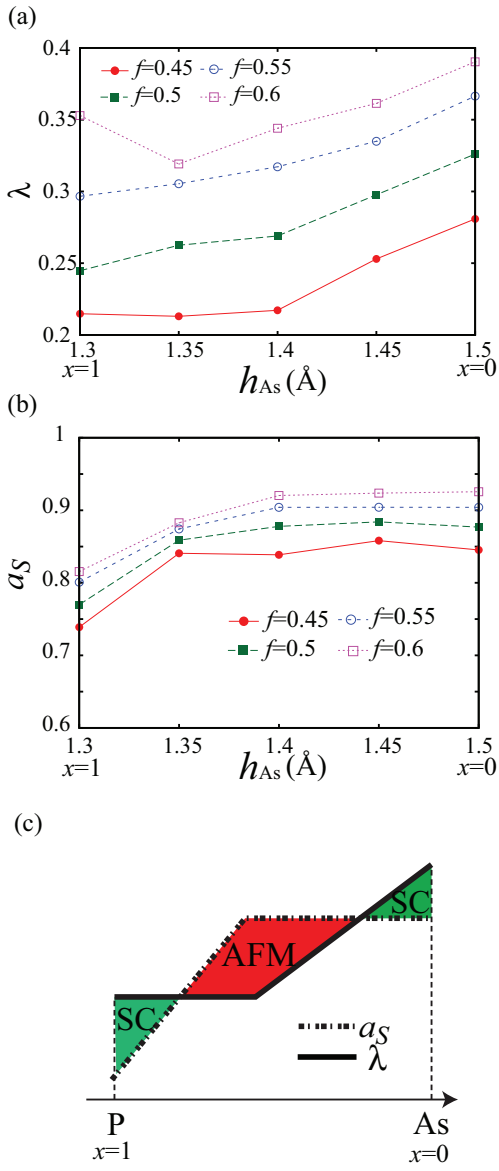

FIG. 10. (Color online) The pnictogen height dependence of (a) the Eliashberg equation eigenvalue and (b) the Stoner factor at $(\pi,0)$ for the hypothetical lattice structure of $Ca_4Al_2O_6Fe_2As_2$. Several values of the reducing factor are taken for comparison. (c) A schematic figure of the x dependence of λ for superconductivity and a_S for antiferromagnetism.

V. CONCLUSION

In the present paper, we studied the origin of the peculiar phase diagram obtained for $Ca_4Al_2O_6Fe_2As_{1-x}P_x$ using a five orbital model constructed from first-principles band calculation. While the inner hole Fermi surface is absent at $x = 0$ (Ref. 24), it is present at $x = 1$, but the orbital character has strong $X^2 - Y^2$ character rather than XZ/YZ as in LaFeAsO. This gives rise to momentum space frustration of the pairing interaction mediated by spin fluctuations, and

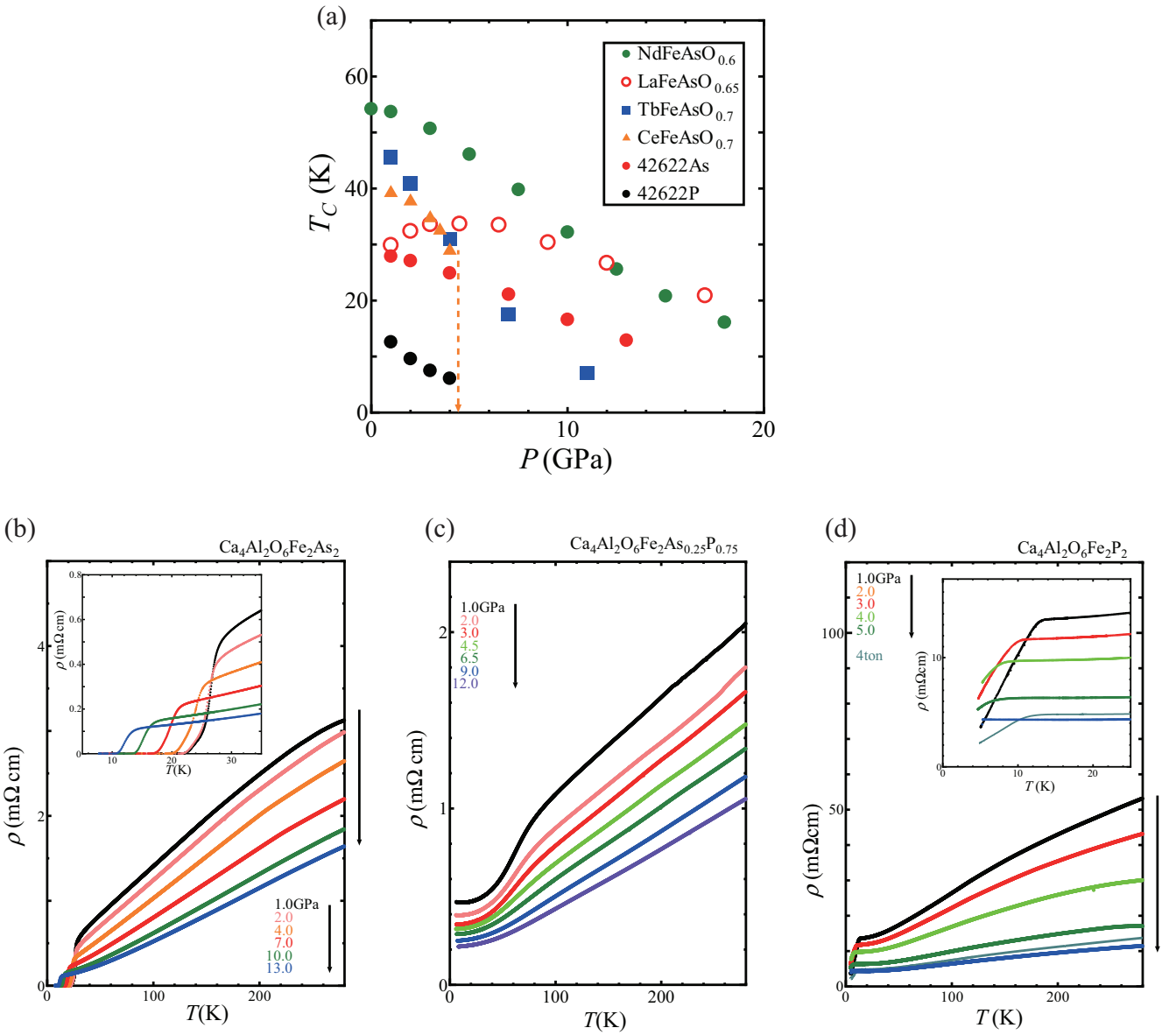

FIG. 11. (Color online) (a) The pressure dependence of the superconducting transition temperature for various materials. The resistivity against pressure for $Ca_4Al_2O_6Fe_2(As_{1-x}P_x)_2$ for (b) $x = 0$, (c) $x = 0.75$ and (d) $x = 1$.

degrades superconductivity. We propose this to be one of the reasons why T_c is not so high in $Ca_4Al_2O_6Fe_2P$ despite the maximized multiplicity of the hole Fermi surface. The frustration effect remains strong even after the inner Fermi surface has disappeared for $x < 1$ because the top of the band with $X^2 - Y^2$ orbital character remains near the Fermi level. At the same time, the disappearance of the most inner hole Fermi surface gives very good nesting of the electron and hole Fermi surfaces due to the equal number of sheets, favoring antiferromagnetism in the intermediate regime of x. Finally, for $x \sim 0$, the top of the band sinks far below the Fermi level, and the frustration effect is reduced, so that superconductivity is favored once again. Although we cannot directly determine which one of the superconductivity and antiferromagnetism wins, the tendency observed in the calculation is at least consistent with the experimental observation, where nodeless and nodal superconducting phases are separated by an antiferromagnetic phase. Finally, we have performed a hydrostatic pressure experiment, which further supports our scenario that superconductivity is suppressed by momentum space frustration in the intermediate x regime.

ACKNOWLEDGMENTS

We are grateful to H. Mukuda, H. Kinouchi, and Y.Kitaoka for fruitful discussions. The numerical calculations were performed at the Supercomputer Center, ISSP, University of Tokyo. This study has been supported by Grants-in-Aid for Scientific Research from JSPS. K.S. acknowledges support from JSPS.

[1]Y. Kamihara, T. Watanabe, M. Hirano, and H. Hosono, J. Am. Chem. Soc. **130**, 3296 (2008).
[2]Z.-A. Ren, L. Wei, Y. Jie, Y. Wei, S. X. Li, Z. Cai, C. G. Can, D. X. Li, S. L. Ling, Z. Fang, and Z. Z. Xian, Chin. Phys. Lett. **25**, 2215 (2008).
[3]K. Kuroki, S. Onari, R. Arita, H. Usui, Y. Tanaka, H. Kontani, and H. Aoki, Phys. Rev. Let. **101**, 087004 (2008).
[4]I. I. Mazin, D. J. Singh, M. D. Johannes, and M. H. Du, Phys. Rev. Lett. **101**, 057003 (2008).
[5]C.-H. Lee, A. Iyo, H. Eisaki, H. Kito, M. T. Fernandez-Diaz, T. Ito, K. Kihou, H. Matsuhata, M. Braden, and K. Yamada, J. Phys. Soc. Jpn. **77**, 083704 (2008).
[6]Y. Mizuguchi and Y. Takano, J. Phys. Soc. Jpn. **79**, 102001 (2010).
[7]H. Kinouchi, H. Mukuda, M. Yashima, Y. Kitaoka, P. M. Shirage, H. Eisaki, and A. Iyo, Phys. Rev. Lett. **107**, 047002 (2011).
[8]K. Ishida, Y. Nakai, and H. Hosono, J. Phys. Soc. Jpn. **78**, 062001 (2009), and references therein.
[9]Y. Nakai, S. Kitagawa, K. Ishida, Y. Kamihara, M. Hirano, and H. Hosono, New J. Phys. **11**, 045004 (2009).
[10]H. Mukuda, N. Terasaki, N. Tamura, H. Kinouchi, M. Yashima, Y. Kitaoka, K. Miyazawa, P. M. Shirage, S. Suzuki, S. Miyasaka, S. Tajima, H. Kito, H. Eisaki, and A. Iyo, J. Phys. Soc. Jpn. **78**, 084717 (2009).
[11]T. Nakano, N. Fujiwara, K. Tatsumi, H. Okada, H. Takahashi, Y. Kamihara, M. Hirano, and H. Hosono, Phys. Rev. B **81**, 100510 (2010).
[12]P. M. Shirage, K. Kihou, C. H. Lee, H. Kito, H. Eisaki, and A. Iyo, Appl. Phys. Lett. **97**, 172506 (2010).
[13]H. Ogino, Y. Matsumura, Y. Katsura, K. Ushiyama, S. Horii, K. Kishio, and J. Shimoyama, Supercond. Sci. Technol. **22**, 075008 (2009).
[14]H. Usui and K. Kuroki, Phys. Rev. B **84**, 024505 (2011).
[15]K. Kuroki, H. Usui, S. Onari, R. Arita, and H. Aoki, Phys. Rev. B **79**, 224511 (2009).
[16]S. Graser, T. A. Maier, P. J. Hirschfeld, and D. J. Scalapino, New J. Phys. **11**, 025016 (2009).
[17]F. Wang, H. Zhai, and D.-H. Lee, Phys. Rev. B **81**, 184512 (2010).
[18]R. Thomale, C. Platt, W. Hanke, and B. A. Bernevig, Phys. Rev. Lett. **106**, 187003 (2011).
[19]D. J. Singh and M.-H. Du, Phys. Rev. Lett. **100**, 237003 (2008).
[20]V. Vildosola, L. Pourovskii, R. Arita, S. Biermann, and A. Georges, Phys. Rev. B **78**, 064518 (2008).
[21]T. Kosugi, T. Miyake, and S. Ishibashi, J. Phys. Soc. Jpn **81**, 014701 (2012).
[22]H. Kinouchi, H. Mukuda, Y. Kitaoka, P. M. Shirage, H. Fujihisa, Y. Gotoh, H. Eisaki, and A. Iyo, Phys. Rev. B **87**, 121101(R) (2013).
[23]P. M. Shirage, K. Kihou, C.-H. Lee, N. Takeshita, H. Eisaki, and A. Iyo, J. Am. Chem. Soc. **134**, 15181 (2012).
[24]T. Miyake, T. Kosugi, S. Ishibashi, and K. Terakura, J. Phys. Soc. Jpn. **79**, 123713 (2010).
[25]S. Baroni, A. Dal Corso, S. de Gironcoli, P. Giannozzi, C. Cavazzoni, G. Ballabio, S. Scandolo, G. Chiarotti, P. Focher, A. Pasquarello, K. Laasonen, A. Trave, R. Car, N. Marzari, and A. Kokalj, http://www.quantum-espresso.org/; Here we adopt the exchange correlation functional introduced by J. P. Perdew, K. Burke, and Y. Wang, Phys. Rev. B **54**, 16533 (1996); and the wave functions are expanded by plane waves up to a cutoff energy of 40 Ry. 8^3 k-point meshes are used with the special points technique by H. J. Monkhorst and J. D. Pack, *ibid.* **13**, 5188 (1976).
[26]N. Marzari and D. Vanderbilt, Phys. Rev. B **56**, 12847 (1997); I. Souza, N. Marzari, and D. Vanderbilt, *ibid.* **65**, 035109 (2001); The Wannier functions are generated by the code developed by A. A. Mostofi, J. R. Yates, N. Marzari, I. Souza, and D. Vanderbilt, http://www.wannier.org/.
[27]H. Usui, K. Suzuki, and K. Kuroki, Supercond. Sci. Technol. **25**, 084004 (2012).
[28]N. E. Bickers, D. J. Scalapino, and S. R. White, Phys. Rev. Lett. **62**, 961 (1989).
[29]T. Dahm and L. Tewordt, Phys. Rev. Lett. **74**, 793 (1995).
[30]T. Miyake, T. Kosugi, S. Ishibashi, and K. Terakura (private communications).
[31]H. Ikeda, J. Phys. Soc. Jpn. **77**, 123707 (2008).
[32]R. Arita and H. Ikeda, J. Phys. Soc. Jpn. **78**, 113707 (2009).
[33]H. Ikeda, R. Arita, and J. Kuneš, Phys. Rev. B **81**, 054502 (2010).
[34]The result given here is slightly different from those presented in our previous paper (Ref. 27). There, the band filling was taken at $n = 6.1$, while in the present paper, the band filling is $n = 6$.